Performance Analysis of RSMA-aided UAV-to-Ground Communications

Thai-Hoc Vu[1], Daniel Benevides da Costa[2], Quoc-Viet Pham[3], and Sunghwan Kim[1]
[1]Department of Electrical, Electronic and Computer Engineering, University of Ulsan, Republic of Korea
[2]Technology Innovation Institute, 9639 Masdar City, Abu Dhabi, United Arab Emirates
[3]School of Computer Science and Statistics, Trinity College Dublin, Dublin 2, D02 PN40, Ireland
Emails: vuthaihoc1995@gmail.com, daniel.costa@tii.ae, viet.pham@tcd.ie, sungkim@ulsan.ac.kr

***Abstract*—This paper investigates the performance of downlink rate-splitting multiple access (RSMA)-aided unmanned aerial vehicle (UAV) communication systems, wherein a multi-antenna UAV exploits RSMA to serve multiple ground users. Considering non-line-of-sight environments, double-shadowed scattering channel modeling is adopted to generically characterize the impacts of mobility and shadowing on UAV-to-ground communications, assuming imperfect successive interference cancellation (SIC). Besides, a unified precoder design is proposed to fully capture the benefits of multi-antenna paradigms. Closed-form expressions for the users' outage probability (OP) and ergodic capacity are derived. In addition, asymptotic analysis is carried out to get further insights into the system design, such as the diversity gain and ergodic slope. Numerical results are presented, and it is shown that: 1) the effects of double-shadowed scattering on the system outage performance can be significantly reduced by increasing the number of antennas installed at the UAV; 2) the imperfect SIC error can be minimized by properly optimizing the power allocation of the common stream; and 3) RSMA provides superior users' ergodic capacity compared to its orthogonal and non-orthogonal multiple access counterparts.**

***Index Terms*—Imperfect successive interference cancellation (SIC), multiple-input single-output (MISO), rate-splitting multiple access (RSMA), unmanned aerial vehicle (UAV).**

I. Introduction

The rapid growth of the Internet-of-things (IoT) introduces challenges for sixth-generation (6G) communication networks [1], particularly in terms of spectral efficiency (SE) to support high data rates services (e.g., telesurgery, autonomous vehicles, and metaverse). To this end, rate-splitting multiple access (RSMA) has emerged as a powerful candidate [2] by leveraging the advantages of linear/non-linear precoding and power multiplexing schemes. Specifically, the transmitter splits the message into common and private parts; the former is encoded into a single or multiple common streams and the latter is encoded separately. Thus, the receivers employ successive interference cancellation (SIC) to separate the common stream from the private streams, while the intended private stream is decoded by treating the residual multi-user interference as noise. In this way, RSMA outperforms conventional multiple access schemes, such as space-division multiple access (SDMA) and non-orthogonal multiple access (NOMA), by providing unique benefits, which include enhanced spectral, energy, and computation efficiency. Over the last years, RSMA has been broadly studied in various multi-antenna communication systems [3]–[5].

Unmanned aerial vehicle (UAV) communications have gained a lot of interest in deploying IoT terrestrial networks since they can provide rapid resiliency to network services (i.e., disaster areas), offload the system in congested situations (viz., urban), and fulfill varied requests (e.g., increased ubiquitous connectivity) [6]. Towards large-scale IoT, the interplay between UAV and RSMA has been explored in different systems. For multiple-input multiple-output (MIMO) systems, UAV relied on RSMA to enhance reliability [7], while assuming multiple-input single-output (MISO) systems, the works in [8] jointly optimized the UAV location, the weighted precoder, and the common rate tolerance to maximize the users' sum rate. For single-input single-output (SISO) systems, the authors of [9] studied the users' outage probability (OP) and the throughput maximization. Further, the ergodic capacity (EC) was evaluated in [10], and in [11] the ergodic sum rate was maximized by jointly optimizing the UAV position, the message power allocation (PA) factors, and the common rate.

It is worth noting that prior works [7]–[11] have mostly focused on line-of-sight (LoS) transmission under the assumption of highly stable mobility scenarios. Nevertheless, in practical environments, UAV-to-ground (U2G) communications are typically hindered by large obstacles, resulting in non-LoS (NLoS) phenomena. Also, due to the unstable movement of the UAV and ground users, and/or changes in local ambient scatterers, the wireless signal is often propagated by multiple reflections, scattering, and diffraction, thereby producing a double shadowing [12]. Although these phenomena are indeed factual views, their overall impact remains untouched, which impels us to undertake this work. In addition, from an information theory perspective, finding an optimal precoder solution in RSMA is a rather complicated task that has yet to be outlined in the literature. To the best of the authors' knowledge, most of the existing works primarily adopted RSMA for single-antenna UAV transmissions, which limits the outstanding benefits of the precoder design to multi-antenna systems. Consequently, inter-user interference cannot be alleviated and the system's performance quality, therefore, is considerably

This work was supported by the Research Program through the National Research Foundation of Korea under Grant NRF-2023R1A2C1003546.

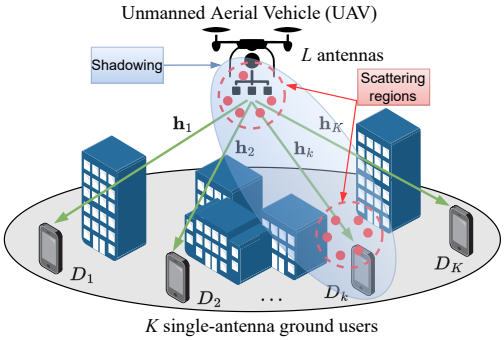

Fig. 1: System model.

deteriorated. Moreover, to guide system designers to gain some practical insights, it is necessary to study the impact of non-ideal SIC receivers.

To fulfill the above research gap, this paper investigates the performance of downlink RSMA-aided U2G communication systems by modeling practical double-shadowing scenarios and non-ideal SIC receiver designs. To simultaneously serve multiple users while fully exploiting the benefits of multi-antenna UAV transmission, the proposed precoder design is formulated in closed-form. Moreover, it is derived the closed-form expressions for the joint probability density functions (PDFs) of the double multipath scattering channels, the double shadowing channels, and the double-shadowed scattering ones. Besides, the moment-generating function (MGF) for the Frobenius norm of the double-shadowed scattering channel is also deduced in closed-form. Based on this, the exact single-integral formulation and the approximated closed-form ones for users' OP and EC are derived. Aiming to guide some technical insights, the asymptotic analyses are also carried out at high signal-to-noise ratio (SNR), wherein users' diversity gain and ergodic slope are deduced. Numerical results are presented to corroborate our derived theoretical analyses and reveal that: 1) the higher number of antenna settings at the UAV yields a lower OP for users; 2) optimizing the PA coefficient for the common message streams can minimize the effect of imperfect SIC on the users' OP; and 3) the users' ECs obtained from RSMA are almost twice those of NOMA and orthogonal multiple access (OMA) counterparts.

II. System Model

Consider a downlink U2G system, as shown in Fig. 1, where a L-antennas UAV adopts RSMA to enhance the transmission rate of K single-antenna ground users (denoted by D_k with $k \in \{1, ..., K\}$). By exploiting the shared codebook scheme, a user message m_k is split into the common part $m_{c,k}$ and the private one $m_{p,k}$, which are then encoded into the respective stream x_c and x_k, with the expectation $\mathbb{E}[|x_c|^2] = \mathbb{E}[|x_k|^2] = 1$. The signal received by the k user over the channel vector $\mathbf{h}_k \in \mathbb{C}^{L\times 1}$ can be expressed as

$$y_k = \mathbf{h}_k^\dagger(\sqrt{\delta_c}\mathbf{w}_c x_c + \sum\nolimits_{k=1}^{k} \sqrt{\delta_k}\mathbf{w}_k x_k)\sqrt{P} + n_k, \quad (1)$$

where P denotes the transmit power of the UAV, δ_c and δ_k denote, correspondingly, the PA factors of x_c and x_k, $\mathbf{w}_c \in \mathbb{C}^{L\times 1}$ and $\mathbf{w}_k \in \mathbb{C}^{L\times 1}$ are the precoding vectors, and $n_k \sim \mathcal{CN}(0, \sigma^2)$ is the additive white Gaussian noise.

By using SIC[1], the k-th user decodes x_c and x_k with the respective signal-to-interference-plus-noise ratio (SINR)

$$\begin{aligned}\gamma_c^k &= \frac{\delta_c P|\mathbf{h}_k^\dagger \mathbf{w}_c|^2}{\delta_k P|\mathbf{h}_k^\dagger \mathbf{w}_k|^2 + \sum_{\bar{k}=1,\bar{k}\neq k}^{K} \delta_{\bar{k}} P|\mathbf{h}_{\bar{k}}^\dagger \mathbf{w}_k|^2 + \sigma^2} \\ &= \frac{\delta_c \bar{\gamma}\|\mathbf{h}_k\|^2}{\delta_k \bar{\gamma}\|\mathbf{h}_k\|^2 + 1}, \end{aligned} \quad (2)$$

$$\begin{aligned}\gamma_p^k &= \frac{\delta_k P|\mathbf{h}_k^\dagger \mathbf{w}_k|^2}{\sum_{\bar{k}=1,\bar{k}\neq k}^{K} \delta_{\bar{k}} P|\mathbf{h}_{\bar{k}}^\dagger \mathbf{w}_k|^2 + \psi_k \delta_c P|\mathbf{h}_k^\dagger \mathbf{w}_c|^2 + \sigma^2} \\ &= \frac{\delta_k \bar{\gamma}\|\mathbf{h}_k\|^2}{\psi_k \delta_c \bar{\gamma}\|\mathbf{h}_k\|^2 + 1}, \end{aligned} \quad (3)$$

where $\psi_k \in [0, 1)$ is the SIC error and $\bar{\gamma} = P/\sigma^2$ is the average SNR. The simplified expressions of $|\mathbf{h}_k^\dagger \mathbf{w}_c|^2$, $|\mathbf{h}_k^\dagger \mathbf{w}_k|^2$, and $|\mathbf{h}_{\bar{k}}^\dagger \mathbf{w}_k|^2$ are obtained from the following design.

A. Precoder Design

For convenience, we define $\mathbf{H} = [\mathbf{h}_1, ..., \mathbf{h}_k, ..., \mathbf{h}_K]$, $\mathbf{W} = [\mathbf{w}_1, ..., \mathbf{w}_k, ..., \mathbf{w}_K]$, $\mathbf{U} = \mathrm{diag}(\|\mathbf{h}_1\|, ..., \|\mathbf{h}_k\|, ..., \|\mathbf{h}_K\|)$, and $\mathbf{Z} = [1_1, ..., 1_k, ..., 1_K]$ as the $L\times K$ channel matrix, the $L\times K$ private precoding matrix, the $K \times K$ diagonal matrix, and the $K \times 1$ all-one vector, respectively. To null the inter-user interference in γ_c^k and γ_p^k, $\mathbf{h}_{\bar{k}}^\dagger \mathbf{w}_k$ should be zero. Thus, each private precoding weight $\mathbf{w}_k$ for the k-th user is orthogonal to every channel vector $\mathbf{h}_{\bar{k}}$ associated with user $\bar{k}$. On another front, γ_p^k is maximized if $\mathbf{h}_k^\dagger \mathbf{w}_k = \|\mathbf{h}_k\|$. Accordingly, the joint orthogonal condition and channel multiplication maximization can be represented as a matrix form $\mathbf{H}^\dagger\mathbf{W} = \mathbf{U}$. By taking into account the right Moore-Penrose pseudo-inverse of $\mathbf{H}^\dagger$, $\mathbf{W}$ can be rearranged to be

$$\mathbf{W} = \mathbf{H}(\mathbf{H}^\dagger\mathbf{H})^{-1}\mathbf{U}. \quad (4)$$

By mapping $\mathbf{W} = [\mathbf{w}_1, ..., \mathbf{w}_k, ..., \mathbf{w}_K]$ with the achieved result above, one can readily obtain $\mathbf{w}_k$. However, for a special case when $K = 2$, the outcome in (4) can be rewritten as

$$\begin{aligned}\mathbf{W} &= \mathbf{H}\frac{(\mathbf{Tr}(\mathbf{H}^\dagger\mathbf{H})\mathbf{I} - \mathbf{H}^\dagger\mathbf{H})}{\det(\mathbf{H}^\dagger\mathbf{H})}\mathbf{U} \\ &= \frac{1}{\det(\mathbf{H}^\dagger\mathbf{H})}\begin{bmatrix} \mathbf{h}_1(\sum_{j=1}^{K}\mathbf{h}_j^H\mathbf{h}_j) - \sum_{j=1}^{K}\mathbf{h}_j(\mathbf{h}_j^H\mathbf{h}_1) \\ \cdots \\ \mathbf{h}_k(\sum_{j=1}^{K}\mathbf{h}_j^H\mathbf{h}_j) - \sum_{j=1}^{K}\mathbf{h}_j(\mathbf{h}_j^H\mathbf{h}_k) \\ \cdots \\ \mathbf{h}_K(\sum_{j=1}^{K}\mathbf{h}_j^H\mathbf{h}_j) - \sum_{j=1}^{K}\mathbf{h}_j(\mathbf{h}_j^H\mathbf{h}_K) \end{bmatrix}^T \mathbf{U}. \end{aligned} \quad (5)$$

By mapping each term above with the previous definition, the closed-form solution for $\mathbf{w}_k$ can be inferred as

$$\mathbf{w}_k = \frac{\|\mathbf{h}_k\|}{\det(\mathbf{H}^\dagger\mathbf{H})}\left[\mathbf{h}_k(\sum_{j=1}^{K}\mathbf{h}_j^H\mathbf{h}_j) - \sum_{j=1}^{K}\mathbf{h}_j(\mathbf{h}_j^H\mathbf{h}_k)\right]. \quad (6)$$

[1]To reduce complexity, it is considered a 1-layer RSMA strategy, which means that common parts are encoded into only one common stream, resulting in only one SIC layer.

Next, γ_c^k is maximized if and only if $\mathbf{h}_k^\dagger \mathbf{w}_c = \|\mathbf{h}_k\|$. Since $\mathbf{h}_k^\dagger \mathbf{w}_k = 0$, $\mathbf{h}_k^\dagger \mathbf{W} = [0, ..., \|\mathbf{h}_k\|, ..., 0]$. Following that, a closed-form representation for $\mathbf{w}_c$ can be inferred as

$$\mathbf{w}_c = \mathbf{W}\mathbf{Z} = \sum_{k=1}^{K} \mathbf{w}_k. \tag{7}$$

B. Channel Modeling

Assuming practical U2G communication, a double-shadowing scenario is considered, where dual-localized scattering regions exist at both the transmitter and receiver, being separated by a large distance. In this context, the channel $[\mathbf{h}_k]_l$, with $l \in \{1, ..., L\}$, follows Nakagami/Inverse Gamma (IG) composite fading [12]: $[\mathbf{h}_k]_l = \mathrm{N}_{k,1}\mathrm{N}_{k,2}\sqrt{\mathrm{I}_{k,1}\mathrm{I}_{k,2}}$, with $\mathrm{N}_{k,j}$ and $\mathrm{I}_{k,j}$ representing, respectively, the multipath fading coefficient subject to Nakagami-m distribution and the shadowing factor following the IG distribution, with $j \in \{1, 2\}$. The corresponding PDFs of $|\mathrm{N}_{k,j}|^2$ and $|\mathrm{I}_{k,j}|$ can be written as

$$f_{|\mathrm{N}_{k,j}|^2}(x) = \frac{(m_{k,j})^{m_{k,j}} x^{m_{k,j}-1}}{\Omega_{k,j}^{m_{k,j}} \Gamma(m_{k,j})} \exp\left(-\frac{m_{k,j} x}{\Omega_{k,j}}\right), \tag{8}$$

$$f_{|\mathrm{I}_{k,j}|}(y) = \frac{\beta_{k,j}^{\alpha_{k,j}}}{\Gamma(\alpha_{k,j}) y^{\alpha_{k,j}+1}} \exp\left(-\frac{\beta_{k,j}}{y}\right), \tag{9}$$

where $m_{k,j}$ and $(\alpha_{k,j} > 1)$ are the distribution's shaping parameter, while $\Omega_{k,j}$ and $\beta_{k,j}$ refer to the scale parameters.

III. Performance Evaluation

A. Channel Statistical Analysis

Letting X and Y be independent non-negative random variables, the PDF of $Z = XY$ is $f_Z(z) = \int_0^\infty f_X(x) f_Y(z/x) \frac{1}{x} dx$. Invoking (8) and (9), the PDFs of $|\mathrm{N}_k|^2 \triangleq |\mathrm{N}_{k,1}|^2 |\mathrm{N}_{k,2}|^2$ and $|\mathrm{I}_k| \triangleq |\mathrm{I}_{k,1}||\mathrm{I}_{k,2}|$ can be, respectively, derived by using the aid of [13, Eqs. (3.471.9) and (9.34.3)] as

$$\begin{aligned} f_{|\mathrm{N}_k|^2}(z) &= \int_0^\infty f_{|\mathrm{N}_{k,1}|^2|}(x) f_{|\mathrm{N}_{k,2}|^2|}(z/x) \frac{1}{x} dx \\ &= \frac{z^{-1}}{\Gamma(m_{k,1})\Gamma(m_{k,2})} G_{0,2}^{2,0}\Big(\frac{m_k}{\Omega_k} z \Big|_{m_{k,1}, m_{k,2}}^{-}\Big), \end{aligned} \tag{10}$$

$$\begin{aligned} f_{|\mathrm{I}_k|}(z) &= \int_0^\infty f_{|\mathrm{I}_{k,1}|^2|}(x) f_{|\mathrm{I}_{k,2}|^2|}(z/x) \frac{1}{x} dx \\ &= \frac{z^{-1}(\beta_k/z)^{\alpha_{k,1}}}{\Gamma(\alpha_{k,1})\Gamma(\alpha_{k,2})} G_{0,2}^{2,0}\Big(\frac{\beta_k}{z} \Big|_{\alpha_{k,2} - \alpha_{k,1}, 0}^{-}\Big), \end{aligned} \tag{11}$$

where $m_k \triangleq m_{k,1} m_{k,2}$, $\Omega_k \triangleq \Omega_{k,1}\Omega_{k,2}$, $\beta_k \triangleq \beta_{k,1}\beta_{k,2}$, and $G_{p,q}^{m,n}(\cdot|\cdot)$ denotes the Meijer's G-function [13, Eq. (9.301)]. Revisiting $f_Z(z)$, the PDF of $|[\mathbf{h}_k]_l|^2$ can be deduced as

$$\begin{aligned} f_{|[\mathbf{h}_k]_l|^2}(z) &= \int_0^\infty f_{|\mathrm{N}_k|^2}(x) f_{|\mathrm{I}_k|}(z/x) \frac{1}{x} dx \\ &= \frac{\tau_k \beta_k^{\alpha_{k,1}}}{z^{\alpha_{k,1}+1}} \int_0^\infty G_{0,2}^{2,0}\Big(\frac{\beta_k x}{z} \Big|_{\alpha_{k,2} - \alpha_{k,1}, 0}^{-}\Big) \\ &\quad \times x^{\alpha_{k,1}-1} G_{0,2}^{2,0}\Big(\frac{m_k}{\Omega_k} x \Big|_{m_{k,1}, m_{k,2}}^{-}\Big) dx \\ &= z^{-1} \tau_k G_{2,2}^{2,2}\Big(\frac{m_k z}{\beta_k \Omega_k} \Big|_{m_{k,1}, m_{k,2}}^{1 - \alpha_{k,2}, 1 - \alpha_{k,1}}\Big), \end{aligned} \tag{12}$$

where $\tau_k \triangleq 1/[\Gamma(m_{k,1})\Gamma(m_{k,2})\Gamma(\alpha_{k,1})\Gamma(\alpha_{k,2})]$ and the last step is obtained thanks to the aid of [14, Eq. (21)]. Recall that $|[\mathbf{h}_k]_l|^2 = |\mathrm{N}_k|^2 |\mathrm{I}_k|$, the MGF of $|[\mathbf{h}_k]_l|^2$, therefore, can be achieved by making the use of [14, Eq. (26)] as

$$\begin{aligned} \mathcal{M}_{|[\mathbf{h}_k]_l|^2}(s) &= \int_0^\infty \exp(sz) f_{|[\mathbf{h}_k]_l|^2}(z) dz \\ &= \tau_k G_{3,3}^{2,3}\Big(\frac{-m_k}{\beta_k \Omega_k s} \Big|_{m_{k,1}, m_{k,2}}^{1, 1 - \alpha_{k,2}, 1 - \alpha_{k,1}}\Big). \end{aligned} \tag{13}$$

Since $\|\mathbf{h}_k\|^2 = \sum_{l=1}^{L} |[\mathbf{h}_k]_l|^2$, its MGF can be written as

$$\mathcal{M}_{\|\mathbf{h}_k\|^2}(s) = \prod_{l=1}^{L} \mathcal{M}_{|[\mathbf{h}_k]_l|^2}(s) = [\mathcal{M}_{|[\mathbf{h}_k]_l|^2}(s)]^L. \tag{14}$$

With the aid of [15, Eq. (8.2.2.30)], the first-order derivative of $\mathcal{M}_{\|\mathbf{h}_k\|^2}(s)$ with respect to s can be expressed as

$$\begin{aligned} \mathcal{M}_{\|\mathbf{h}_k\|^2}^{(1)}(s) = -\frac{L}{s} \left[G_{3,3}^{2,3}\Big(\frac{-m_k}{\beta_k \Omega_k s} \Big|_{m_{k,1}, m_{k,2}}^{1, 1 - \alpha_{k,2}, 1 - \alpha_{k,1}}\Big)\right]^{L-1} \\ \tau_k^L G_{4,4}^{2,4}\Big(\frac{-m_k}{\beta_k \Omega_k s} \Big|_{m_{k,1}, m_{k,2}, 1}^{0, 1, 1 - \alpha_{k,2}, 1 - \alpha_{k,1}}\Big). \end{aligned} \tag{15}$$

B. Outage Performance Analysis

The outage event can be defined as a situation where the instantaneous rate achieved by users of any link falls below the minimum target data rate. Denote by R_c and R_k the minimum target data rates in [bit/s/Hz] for decoding x_c and x_k, respectively. By using the complementary outage event, the OP of the k-th user can be, mathematically, formulated as

$$\begin{aligned} P_{\mathrm{out}}^k &= 1 - \Pr[\log_2(1 + \gamma_c^k) \geq R_c, \log_2(1 + \gamma_p^k) \geq R_k] \\ &= 1 - \Pr[\gamma_c^k \geq \bar{\gamma}_c, \gamma_k \geq \bar{\gamma}_k] = 1 - \Pr[\bar{\gamma}\|\mathbf{h}_k\|^2 \geq \epsilon] \\ &= \frac{1}{2\pi i} \int_{\varrho - i\infty}^{\varrho + i\infty} \frac{1}{s} \mathcal{M}_{\bar{\gamma}\|\mathbf{h}_k\|^2}(-s) \exp(\epsilon s)\, ds, \end{aligned} \tag{16}$$

where $\Pr[\cdot]$ is the probability operation, $\bar{\gamma}_c = 2^{R_c} - 1$, $\bar{\gamma}_k = 2^{R_k} - 1$, $\epsilon \triangleq \max\{\bar{\gamma}_c/(\delta_c - \bar{\gamma}_c\delta_k), \bar{\gamma}_k/(\delta_k - \bar{\gamma}_k\delta_c\psi_k)\}$, $i = \sqrt{-1}$, and ϱ is selected from the region of convergence of the integral in the complex plane s. Note that the above expression exists if and only if $\delta_c - \bar{\gamma}_c\delta_k > 0$; otherwise, $P_{\mathrm{out}}^k = 1$.

Theorem 1: *Using linear transformations $\mathcal{M}_{\bar{\gamma}\|\mathbf{h}_k\|^2}(s) = \mathcal{M}_{\|\mathbf{h}_k\|^2}(s\bar{\gamma})$, the OP of the k-th user can be written in terms of the MGF of $|[\mathbf{h}_k]_l|^2$ as*

$$P_{\mathrm{out}}^k = \frac{1}{2\pi i} \int_{\varrho - i\infty}^{\varrho + i\infty} \frac{1}{s} \underbrace{\exp(\epsilon s) \left[\mathcal{M}_{|[\mathbf{h}_k]_l|^2}(-s\bar{\gamma})\right]^L}_{\Xi(s)} ds. \tag{17}$$

The result above can easily be attained via standard computing software, MATLAB or Wolfram MATHEMATICA, when evaluating the modulus of output complex numbers. However, the form of $\Xi(s)$ involving the Meijer G-function may increase the computational burden of the numerical integration. For this reason, (17) is further considered with two transformation steps: 1) $y = s$ and 2) $y = \varrho\sqrt{1 - x^2}/x$, resulting in

$$P_{\mathrm{out}}^k \overset{1)}{=} \frac{1}{2\pi} \int_{-\infty}^{\infty} \frac{\Xi(\varrho + iy)}{\varrho + iy} dy$$

$$= \frac{1}{2\pi} \int_{-\infty}^{\infty} \frac{\varrho \Re\{\Xi(\varrho+iy)\} + y\Im\{\Xi(\varrho+iy)\}}{\varrho^2+y^2} dy$$

$$\overset{2)}{=} \frac{1}{2\pi} \int_{-1}^{1} \left[\frac{\Re\{\Xi\big(\varrho + i\varrho\frac{\sqrt{1-x^2}}{x}\big)\} + }{\frac{\sqrt{1-x^2}}{x}\Im\{\Xi\big(\varrho + i\varrho\frac{\sqrt{1-x^2}}{x}\big)\}} \right] \frac{dx}{\sqrt{1-x^2}}. \quad (18)$$

Proposition 1: *By utilizing the Gauss–Chebyshev quadrature (GCQ) rule for* (18) *with an even number N of nodes, the OP of the k-th user can be approximated as [16, Eq. (9B.15)]*

$$\bar{P}_{\text{out}}^k = \frac{1}{2N} \sum_{n=1}^{N} \begin{pmatrix} \Re\{\Xi\big(\varrho + i\varrho\theta_n\big)\} + \\ \theta_n \Im\{\Xi\big(\varrho + i\varrho\theta_n\big)\} \end{pmatrix} + \varepsilon(N), \quad (19)$$

where $\theta_n = \tan([2n-1]\pi/[4N])$ and $\varepsilon(N)$ is an error term.

Proposition 1 shows that the approximated result in (19) is particularly efficient from the computational point of view since $\big(\varrho + i\varrho\theta_n\big)$ needs to be calculated only once for each N. Consequently, the users' OP can be readily obtained without making any computational burden compared to the integral in (17) that involves infinite complex boundary conditions.

At high SNR regime (i.e., $\bar{\gamma} \to \infty$), by using [13, Eq. (9.33)], $\mathcal{M}_{|[\mathbf{h}_k]_l|^2}(-s\bar{\gamma})$ can be asymptotically shown as

$$\left(\frac{m_k}{\beta_k \Omega_k \bar{\gamma}}\right)^{m_{k,1}} \sum_{r=0}^{\infty} \frac{\tau_k}{r!} G_{3,3}^{2,3}\left(\frac{1}{s}\middle| \begin{matrix} 1, 1-\alpha_{k,2}, 1-\alpha_{k,1} \\ m_{k,1}+r, m_{k,2} \end{matrix}\right).$$

Accordingly, (17) can be asymptotically written as

$$P_{\text{out}}^k \simeq \frac{1}{2\pi i}\left(\frac{m_k}{\beta_k \Omega_k \bar{\gamma}}\right)^{m_{k,1}L} \int_{\varrho - i\infty}^{\varrho + i\infty} \frac{1}{s} \exp(\epsilon s) \left[\sum_{r=0}^{\infty} \frac{\tau_k}{r!} \times G_{3,3}^{2,3}\left(\frac{1}{s}\middle| \begin{matrix} 1, 1-\alpha_{k,2}, 1-\alpha_{k,1} \\ m_{k,1}+r, m_{k,2} \end{matrix}\right)\right]^L ds. \quad (20)$$

Corollary 1: *Eq.* (20) *shows that $\hat{P}_{\text{out}}^k \propto (1/\bar{\gamma})^{m_{k,1}L}$. Therefore, the diversity gain of users is $m_{k,1}L$.*

C. Ergodic Capacity Analysis

The users' ECs (bit/s/Hz) achieved by the common and private rate streams can be written as

$$C_c^k = \mathbb{E}\{\log_2(1+\gamma_c^k)\} = \mathbb{E}\left\{\log_2\left(\frac{1+\bar{\gamma}(\delta_c+\delta_k)\|\mathbf{h}_k\|^2}{1+\bar{\gamma}\delta_k\|\mathbf{h}_k\|^2}\right)\right\}$$

$$= \int_0^{\infty} \begin{pmatrix} \log_2(1+z) f_{\bar{\gamma}(\delta_c+\delta_k)\|\mathbf{h}_k\|^2}(z) \\ -\log_2(1+z) f_{\bar{\gamma}\delta_k\|\mathbf{h}_k\|^2}(z) \end{pmatrix} dz, \quad (21)$$

$$C_p^k = \mathbb{E}\{\log_2(1+\gamma_p^k)\} = \mathbb{E}\{\log_2\left(\frac{1+\bar{\gamma}(\delta_k+\delta_c\psi_k)\|\mathbf{h}_k\|^2}{1+\bar{\gamma}\delta_c\psi_k\|\mathbf{h}_k\|^2}\right)\}$$

$$= \int_0^{\infty} \begin{pmatrix} \log_2(1+z) f_{\bar{\gamma}(\delta_k+\delta_c\psi_k)\|\mathbf{h}_k\|^2}(z) \\ -\log_2(1+z) f_{\bar{\gamma}\delta_c\psi_k\|\mathbf{h}_k\|^2}(z) \end{pmatrix} dz. \quad (22)$$

To solve (21) and (22), we consider the following two identities

$$\xi \triangleq \log_2(1+X) = \frac{1}{\ln(2)} \int_0^1 \frac{X}{1+yX} dy.$$

$$\frac{X}{X+\eta} = \int_0^{\infty} X \exp(-Xs)\exp(-\eta s) ds.$$

By taking the above expectation, one can get

$$\mathbb{E}\{\xi\} = \frac{1}{\ln(2)} \int_0^1 \frac{1}{y}\Big[\int_0^{\infty} X \exp(-Xs) \exp\Big(-\frac{s}{y}\Big) ds\Big] dy$$

$$= \frac{1}{\ln(2)} \int_0^1 \frac{1}{y}\Big[-\int_0^{\infty} \frac{\partial \mathcal{M}_X(-s)}{\partial s} \exp\Big(-\frac{s}{y}\Big) ds\Big] dy$$

$$= \frac{1}{\ln(2)} \int_0^{\infty} \mathcal{M}_X^{(1)}(-s)\Big[-\int_0^1 \frac{1}{y}\exp\Big(-\frac{s}{y}\Big) dy\Big] ds$$

$$= \frac{1}{\ln(2)} \int_0^{\infty} \mathcal{M}_X^{(1)}(-s)\text{Ei}(-s) ds, \quad (23)$$

where $\text{Ei}(\cdot)$ is the exponential integral function [13, Eq. (8.211.1)]. Let $T \in \{\bar{\gamma}(\delta_c+\delta_k), \bar{\gamma}\delta_k, \bar{\gamma}(\delta_k+\psi_k\delta_c), \bar{\gamma}\psi_k\delta_c\}$. Using $\mathcal{M}_{T\|\mathbf{h}_k\|^2}^{(1)}(s) = -T\mathcal{M}_{\|\mathbf{h}_k\|^2}^{(1)}(sT)$, and invoking (23), one can get the following theorem.

Theorem 2: *C_c^k in* (21) *and C_p^k in* (23) *can be written, respectively, in terms of the MGF of $\|\mathbf{h}_k\|^2$ as*

$$C_c^k = \int_0^{\infty} \frac{\text{Ei}(-s)}{\ln(2)} [-\bar{\gamma}(\delta_c+\delta_k)\mathcal{M}_{\|\mathbf{h}_k\|^2}^{(1)}(-s\bar{\gamma}(\delta_c+\delta_k)) + \bar{\gamma}\delta_k \mathcal{M}_{\|\mathbf{h}_k\|^2}^{(1)}(-s\bar{\gamma}\delta_k)] ds, \quad (24)$$

$$C_p^k = \int_0^{\infty} \frac{\text{Ei}(-s)}{\ln(2)} [-\bar{\gamma}(\delta_k+\delta_c\psi_k)\mathcal{M}_{\|\mathbf{h}_k\|^2}^{(1)}(-s\bar{\gamma}(\delta_k+\delta_c\psi_k)) + \bar{\gamma}\delta_c\psi_k \mathcal{M}_{\|\mathbf{h}_k\|^2}^{(1)}(-s\bar{\gamma}\delta_c\psi_k)] ds. \quad (25)$$

Theorem 2 shows two positive aspects: (i) the ECs are a real number and (ii) the ECs can be represented by a single integral composed of $\mathcal{M}_{\|\mathbf{h}_k\|^2}^{(1)}(\cdot)$ in (15) and a built-in function $\text{Ei}(\cdot)$, which allow us to readily numerically evaluate the users' exact EC without any extra effort. However, it might be interesting to study whether any simple solution with low complexity is found. Using $s^2 + 1/2 = 1/(1+x)$ and letting $\Phi(s,t_1,t_2) \triangleq \text{Ei}(-s)[-t_1\mathcal{M}_{\|\mathbf{h}_k\|^2}(-st_1) + t_2\mathcal{M}_{\|\mathbf{h}_k\|^2}(-st_2)]$, (24) and (25) can be rewritten, respectively, as

$$C_c^k = \frac{1}{\ln(2)} \int_{-1}^{1} \frac{\Phi\left(\sqrt{\frac{1-x}{2(1+x)}}, \bar{\gamma}(\delta_c+\delta_k), \bar{\gamma}\delta_k\right)}{\sqrt{2}(1+x)\sqrt{1-x^2}} dx, \quad (26)$$

$$C_p^k = \frac{1}{\ln(2)} \int_{-1}^{1} \frac{\Phi\left(\sqrt{\frac{1-x}{2(1+x)}}, \bar{\gamma}(\delta_k+\delta_c\psi_k), \bar{\gamma}\delta_c\psi_k\right)}{\sqrt{2}(1+x)\sqrt{1-x^2}} dx. \quad (27)$$

Proposition 2: *By using the GCQ rule, C_c^k in* (26) *and C_p^k in* (27) *can efficiently be approximated, respectively, as*

$$\bar{C}_c^k = \frac{1}{\ln(2)} \sum_{q=1}^{Q} \frac{\pi\Phi\left(\sqrt{\frac{1-\omega_q}{2(1+\omega_q)}}, \bar{\gamma}(\delta_c+\delta_k), \bar{\gamma}\delta_k\right)}{Q\sqrt{2}(1+\omega_q)}, \quad (28)$$

$$\bar{C}_p^k = \frac{1}{\ln(2)} \sum_{q=1}^{Q} \frac{\pi\Phi\left(\sqrt{\frac{1-\omega_q}{2(1+\omega_q)}}, \bar{\gamma}(\delta_k+\delta_c\psi_k), \bar{\gamma}\delta_c\psi_k\right)}{Q\sqrt{2}(1+\omega_q)}, \quad (29)$$

where $\omega_q = \cos((2q-1)\pi/[2Q])$.

At high SNR regime (i.e., $\bar{\gamma} \to \infty$), (21) and (22) can be asymptotically quantified, respectively, as

$$C_c^k = \mathbb{E}\{\log_2(1+\gamma_c^k)\} \overset{\bar{\gamma}\to\infty}{\simeq} \log_2\left(\frac{\delta_c+\delta_k}{\delta_k}\right), \tag{30}$$

$$C_p^k = \mathbb{E}\{\log_2(1+\gamma_p^k)\} \overset{\bar{\gamma}\to\infty}{\simeq} \log_2\left(\frac{\delta_k+\delta_c\psi_k}{\delta_c\psi_k}\right). \tag{31}$$

As can be clearly seen, the common and private ECs become saturated at high SNR regime, which means that increasing $\bar{\gamma}$ does not bring any performance improvement. This also sheds light on the fact that the user's ergodic slope is zero.

IV. Numerical Results and Discussions

This section aims to validate the theoretical analyses (theory) developed in Section III via Monte-Carlo simulations (sim.) as well as to highlight useful insights. All experiments are realized with 10^4 channels. Unless stated explicitly, the parameters are set as follows. Normalized networks include UAV located at $S(0,0,1)$ and three users ($K=3$) positioned at $D_1(0,0.2,0)$, $D_2(-0.5,-0.2,0)$, and $D_3(0.3,-0.4,0)$. Channel parameters comprise $m_{k,1}=2.1$, $m_{k,2}=m_{k,1}+0.3$, $\alpha_{k,1}=1.1$, $\alpha_{k,2}=\alpha_{k,1}+0.5$ [12], $\beta_{k,i}=1$, and $\Omega_{k,i}=d_{\mathrm{SD}_k}^{-\mathtt{path}}$, where the standardized distance from UAV to users is $d_{\mathrm{SD}_k}=\sqrt{(x_{\mathrm{S}}-x_{\mathrm{D}_k})^2+(y_{\mathrm{S}}-y_{\mathrm{D}_k})^2+(z_{\mathrm{S}}-z_{\mathrm{D}_k})^2}$ and $\mathtt{path}=2.7$ is the pathloss exponent. Other parameters are set as: $L=4$, $\delta_c=0.4$, $\delta_k=k(1-\delta_c)/(2K)$, $\psi_k=0.05$, $R_c=0.5$ [bit/s/Hz], $R_k=1$ [bit/s/Hz], and $\varrho=1/2$.

Fig. 2 displays the users' OPs in terms of shape parameters $m_{k,1}$ and $\alpha_{k,1}$ under different operating environments[2]. Fig. 2(a) shows that as $m_{k,1}$ increases, the OP improves due to decreasing the impact of multipath channels. Besides, the user's OPs in the DS case are the worst due to the shadowing occurring in two scattering zones around the UAV and users. In the meanwhile, the other cases with either shadowing or multipath channels appear in only one of the two regions. As a consequence, these also lead to the increasing OP gaps between DS and SS and between DS and SC as $m_{k,1}$ increases, whereas that of between DS and DC is kept stable due to the same multipath channel effect. In Fig. 2(b), as $\alpha_{k,1}$ increase, the OP performance has strongly deteriorated due to increasing shadowing effects.

To diminish the influence of DS phenomena, Fig. 3 investigates the users' OPs against the average SNR $\bar{\gamma}$ in the three cases of antennas installed at the UAV. As observed, the users' OPs improve significantly with the increase in $\bar{\gamma}$ and L. This is because increasing $\bar{\gamma}$ yields better signal strength reception, while for L, users receive more channel gain enhancement provided in (2) and (3), showing the superiority of RSMA with the multi-antenna systems. Besides, the figure also confirms that the simulation results accurately match with the theory curves produced through numerical integration of (17), where the term boundaries are set to be "$\varrho \pm i5$", and also greatly

[2]Note that in channels $[\mathbf{h}_k]_l$ modelling, "DS", "SS", "DC", and "SC" means double-shadowing, double-scattering (without $\mathrm{I}_{k,2}$), single-scattering (without $\mathrm{N}_{k,2}$), and shadowing-scattering (only $\mathrm{N}_{k,1}$ and $\mathrm{I}_{k,1}$), respectively.

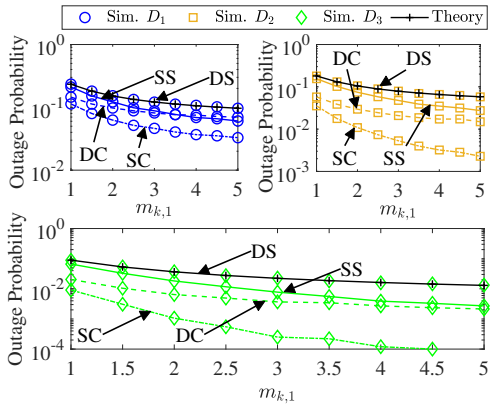

(a) Effects of shape fading parameter $m_{k,1}$.

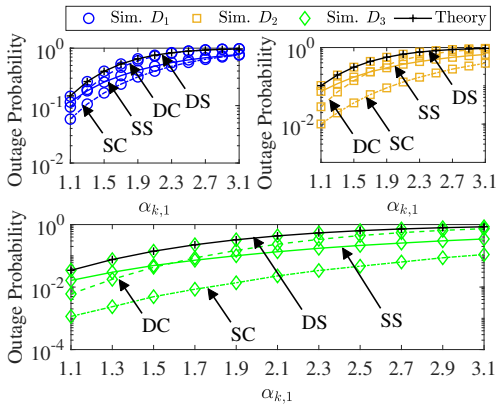

(b) Effects of shape fading parameter $\alpha_{k,1}$.

Fig. 2: OP against $m_{k,1}$ and $\alpha_{k,1}$ with $\bar{\gamma}=7.5$ dB.

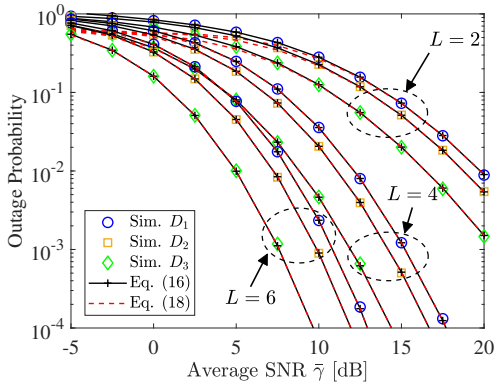

Fig. 3: OP against average SNR $\bar{\gamma}$.

align with the approximated curves produced through (19) using $N=30$, which in turn verifies our analyses.

Next, Fig. 4 depicts the users' OPs as a function of δ_c while varying non-ideal SIC errors. As observed, the OPs of users are indeed convex functions with respect to δ_c. Moreover, as ψ_k increases, the users' OPs increase due to increasing residual interference during SIC. Obviously, there is an optimal δ_c^* which cannot only improve the users' OPs but

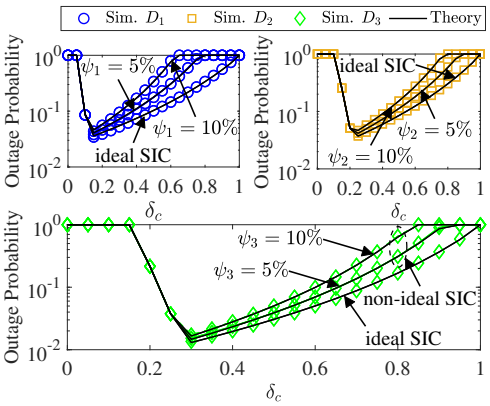

Fig. 4: OP against δ_c with $\bar{\gamma} = 7.5$ dB.

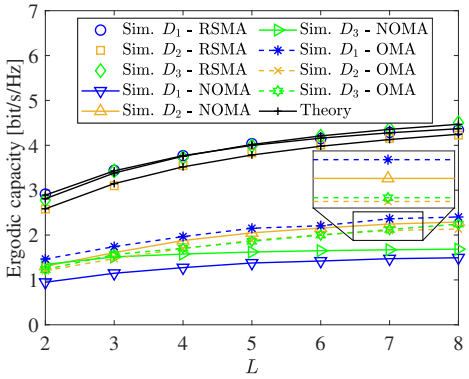

Fig. 5: EC against L with $\bar{\gamma} = 7.5$ dB.

also alleviate the negative effect of non-ideal SIC design. With the developed open-form expressions in hand, the optimal solution for δ_c^* can be easily obtained through one-dimensional search approaches with relatively low complexity.

Fig. 5 investigates the users' ECs (i.e., $C_c^k + C_p^k$) against L while also comparing it with the NOMA and OMA counterparts[3]. As observed, the theory curves produced through numerical integration of (24) and (25), where the upper bound value is set to be "5", show perfect agreement with the simulation results. In addition, as L increases, the users' ECs improve significantly. Moreover, it has been shown that RSMA yields better users' ECs than its counterpart (approximately double times) due to the additional common EC.

V. Conclusions

This paper has provided a generalized analysis framework of downlink RSMA-aided multi-antenna U2G communication systems, wherein a novel precoder solution for multi-antenna UAV transmission was formulated based on the correlation of the users' channel characteristics. Accordingly, the OP and EC of users were derived in terms of open-form single-integral expressions using MGF approaches and the approximate closed-form expressions using GCQ rules, thus reducing the computational complexity. In addition, the asymptotic OP and EC were analyzed to glean some insights into real-world scenarios, such as the diversity gain and ergodic slope. In particular, numerical results revealed that: 1) the developed theoretical analyses aligned closely with the simulation results; 2) increasing the number of antennas at the UAV reduces the effects of double shadowing phenomena significantly; 3) optimizing the common PA coefficient can minimize the impact of non-ideal SIC receiver designs; and 4) RSMA outperformed NOMA and OMA in terms of the users' EC.

[3]In NOMA, the PA coefficients for the signals of D_1, D_2, and D_3 are, respectively, set as 0.1, 0.2, and 0.7. For OMA, all users are served by full transmit power according to orthogonal scheduling times.

References

[1] A. M. Aslam, R. Chaudhary, A. Bhardwaj, I. Budhiraja, N. Kumar *et al.*, "Metaverse for 6G and beyond: The next revolution and deployment challenges," *IEEE Internet Things Mag.*, vol. 6, no. 1, pp. 32–39, Mar. 2023.

[2] Y. Mao, O. Dizdar, B. Clerckx, R. Schober, P. Popovski *et al.*, "Rate-splitting multiple access: Fundamentals, survey, and future research trends," *IEEE Commun. Surv. Tutorials*, vol. 24, no. 4, pp. 2073–2126, July 2022.

[3] X. Ou, X. Xie, H. Lu, and H. Yang, "Resource allocation in MU-MISO rate-splitting multiple access with SIC errors for URLLC services," *IEEE Trans. Commun.*, vol. 71, no. 1, pp. 229–243, Jan. 2023.

[4] R. C. Loli, O. Dizdar, B. Clerckx, and C. Ling, "Model-based deep learning receiver design for rate-splitting multiple access," *IEEE Trans. Wireless Commun.*, Apr. 2023, in press.

[5] M. Wu, Z. Gao, Y. Huang, Z. Xiao, D. W. K. Ng *et al.*, "Deep learning-based rate-splitting multiple access for reconfigurable intelligent surface-aided tera-hertz massive MIMO," *IEEE J. Sel. Areas Commun.*, vol. 41, no. 5, pp. 1431–1451, May 2023.

[6] N.-N. Dao, Q.-V. Pham, N. H. Tu, T. T. Thanh, V. N. Q. Bao *et al.*, "Survey on aerial radio access networks: Toward a comprehensive 6G access infrastructure," *IEEE Commun. Surv. Tutorials*, vol. 23, no. 2, pp. 1193–1225, Feb. 2021.

[7] T.-H. Vu, T. Q. Duong, T.-H. Khuat, T. H. Nguyen, and S. Kim, "Short-packet communication for cooperative UAV-based MIMO systems with rate splitting multiple access," in *Proc. IEEE Int. Conf. Commun. Elec. (ICCE)*, Jul. 2022, pp. 113–117.

[8] W. Jaafar, S. Naser, S. Muhaidat, P. C. Sofotasios, and H. Yanikomeroglu, "On the downlink performance of RSMA-based UAV communications," *IEEE Trans. Veh. Technol.*, vol. 69, no. 12, pp. 16 258–16 263, Dec. 2020.

[9] S. K. Singh, K. Agrawal, K. Singh, and C.-P. Li, "Outage probability and throughput analysis of UAV-assisted rate-splitting multiple access," *IEEE Wireless Commun. Lett.*, vol. 10, no. 11, pp. 2528–2532, Nov. 2021.

[10] S. K. Singh, K. Agrawal, K. Singh, and C.-P. Li, "Ergodic capacity and placement optimization for RSMA-enabled UAV-assisted communication," *IEEE Syst. J.*, vol. 17, no. 2, pp. 2586–2589, Jun. 2023.

[11] S. K. Singh, K. Agrawal, K. Singh, Y.-M. Chen, and C.-P. Li, "Performance analysis and optimization of RSMA enabled UAV-aided IBL and FBL communication with imperfect SIC and CSI," *IEEE Trans. Wireless Commun.*, vol. 22, no. 6, pp. 3714–3732, Jun. 2023.

[12] P. S. Bithas, V. Nikolaidis, A. G. Kanatas, and G. K. Karagiannidis, "UAV-to-ground communications: Channel modeling and UAV selection," *IEEE Trans. Commun.*, vol. 68, no. 8, pp. 5135–5144, May 2020.

[13] A. Jeffrey and D. Zwillinger, *Table of integrals, series, and products*. Elsevier, 2007.

[14] V. S. Adamchik and O. I. Marichev, "The algorithm for calculating integrals of hypergeometric type functions and its realization in REDUCE system," in *ISSAC '90: Proc. Int. Symp. Symbolic Algebraic Comput.*, New York, NY, USA, July 1990, pp. 212–224.

[15] A. P. Prudnikov, Y. A. Brychkov, and O. I. Marichev, *Integrals and Series*. Amsterdam, The Netherlands: Gordon Breach Sci, 1990, vol. 3.

[16] M. K. Simon and M.-S. Alouini, *Digital communication over fading channels*. Wiley-IEEE Press, 2005.